Unseen companions of V Hya inferred from periodic ejections

Jesus M. Salas,[1]★ Smadar Naoz [1,2] Mark R. Morris[1] and Alexander P. Stephan[1,2]

[1]*Department of Physics & Astronomy, University of California, Los Angeles, CA 90095, USA*
[2]*Department of Physics and Astronomy, Mani L. Bhaumik Institute for Theoretical Physics, University of California, Los Angeles, CA 90095, USA*

ABSTRACT

A recent study using *Hubble Space Telescope* observations found periodic, high-speed, collimated ejections (or 'bullets') from the star V Hya. The authors of that study proposed a model associating these bullets with the periastron passage of an unseen, substellar companion in an eccentric orbit and with an orbital period of ∼8 yr. Here we propose that V Hya is part of a triple system, with a substellar companion having an orbital period of ∼8 yr, and a tertiary object on a much wider orbit. In this model, the more distant object causes high-eccentricity excitations on the substellar companion's orbit via the Eccentric Kozai–Lidov mechanism. These eccentricities can reach such high values that they lead to Roche-lobe crossing, producing the observed bullet ejections via a strongly enhanced accretion episode. For example, we find that a ballistic bullet ejection mechanism can be produced by a brown-dwarf-mass companion, while magnetically driven outflows are consistent with a Jovian-mass companion. Finally, we suggest that the distant companion may reside at few a hundred astronomical units on an eccentric orbit.

Key words: binaries: general – stars: evolution – stars: kinematics and dynamics.

1 INTRODUCTION

Observations from the *Hubble Space Telescope* (*HST*) over the past two decades have revealed an enormous complexity and diversity of structure in planetary nebulae (PNe; Balick & Frank 2002; Sahai, Morris & Villar 2011). *HST* surveys have revealed that more than half of PNe are bipolar or multipolar whereas mass-loss during the AGB phase is mostly spherical. This led Sahai & Trauger (1998) to propose that high-speed, collimated (jet-like) outflows during the late AGB phase that can change their orientation could be the reason behind the asymmetric morphology of PNe. These jets could be driven by interactions with a binary companion (Morris 1987); however, direct evidence supporting this idea has been lacking.

The carbon star V Hya is one example where there exists evidence for high-speed, collimated outflows (Lloyd Evans 1991; Knapp, Jorissen & Young 1997; Sahai & Trauger 1998; Sahai et al. 2003; Hirano et al. 2004; Sahai, Sugerman & Hinkle 2009). A recent study by Sahai, Scibelli & Morris (2016) presents new *HST* observations that span more than a decade and provide, with an unprecedented and detailed view, the extended history and characteristics of the bullet-like ejections from V Hya. Their data show that these high-speed (∼200–250 km s^{-1}) bullets are ejected once every ∼8.5 yr, and that the axis of ejection flip-flops around a roughly eastern direction, both in and perpendicular to the sky plane.

To account for this phenomenon, Sahai et al. (2016) proposed a model in which the bullets are associated with the periastron passage of a binary companion in an eccentric orbit with an orbital period of ∼8.5 yr. The bullets are likely ejected from an accretion disc formed around the companion that results from the gravitational capture of matter levitated into the primary's wind-formation zone, and perhaps directly from the primary's pulsating atmosphere. However, this hypothesis faces the difficulty that tidal forces between binary companions tend to shrink and circularize their orbits, or even cause mergers. To overcome this problem, we here propose a more elaborated model in which V Hya is part of a triple system. In such a system, a relatively distant third object can impose an eccentric orbit on the inner companion, and even lead to Roche-limit crossing, thus allowing the inner companion to accrete and eject mass.

Studies of stellar populations have shown that multiple star systems are very common, with ∼50 per cent of Sun-like stars having binary companions, and even higher fractions (∼70 per cent) are found for higher-mass stars (e.g. Raghavan et al. 2010). Moreover, it seems that many of these binaries are in triples or higher multiples. For example, Tokovinin (1997a) showed that ∼40 per cent of short-period binary stars with a low-mass (∼0.5–1.5 M$_\odot$) primary have at least one additional companion. Furthermore, among contact binaries it seems that about 42 per cent are in a triple configuration (e.g. Pribulla & Rucinski 2006). These and many other observational endeavours have revealed that triple star systems are common (e.g. Tokovinin 1997b; Tokovinin et al. 2006; Eggleton, Kisseleva-Eggleton & Dearborn 2007; Griffin 2012. See also Tokovinin 2008, 2014a,b).

★ E-mail: jesusms@astro.ucla.edu

Dynamical stability considerations dictate that triple systems must be hierarchical in scale, in which the ('inner') binary is orbited by a third body on a much wider ('outer') orbit. In this set-up, the inner binary undergoes large-amplitude eccentricity and inclination oscillations due to the 'Eccentric Kozai-Lidov' (EKL) mechanism (Kozai 1962; Lidov 1962. For a review, see Naoz 2016). These eccentricity excitations can drive the inner binary to have very small pericenter distances and even to merge (e.g. Naoz & Fabrycky 2014; Prodan, Antonini & Perets 2015; Naoz 2016; Stephan et al. 2016; Stephan, Naoz & Zuckerman 2017; Stephan, Naoz & Gaudi 2018).

The star V Hya is currently in its AGB stage with a mass of ∼1–2 M$_\odot$ and a radius of ∼2 au (see Zhao-Geisler et al. 2012). The rapid evolution of an AGB star in a triple system can play a major role in the dynamical evolution of such a system (e.g. Perets & Kratter 2012; Shappee & Thompson 2013; Michaely & Perets 2016; Naoz et al. 2016; Stephan et al. 2016; Toonen, Hamers & Portegies Zwart 2016; Stephan et al. 2017, 2018). For example, as the AGB star loses mass, it can reduce the separation ratio between the inner and outer orbits, thus re-triggering EKL eccentricity excitations (Shappee & Thompson 2013). In addition, as the star expands, tidal forces become more efficient since tides are highly sensitive to the stellar radius.

In particular for the V Hya system, EKL combined with post-main-sequence stellar evolution can drive the inner binary to very high eccentricities and even cause it to undergo Roche-lobe crossing, inducing the secondary object to accrete material from its companion, and perhaps eject some of this material from an accretion disc (Sahai et al. 2016). The mechanism we introduce here thus could explain the observed ejections from V Hya.

This paper is organized as follows. In Section 2 we describe the code and numerical set-up. Our results are shown in Section 3. A discussion of the implications of our model is given in Section 4, and we conclude in Section 5.

2 NUMERICAL METHODS

2.1 Stellar evolution and three-body dynamics

We solve the secular equations for a hierarchical triple system up to the octupole level of approximation (as described in Naoz et al. 2013a; Naoz 2016), including general relativistic effects for both the inner and outer orbits (Naoz et al. 2013b) and static tides for both members of the stellar binary (following Hut 1980; Eggleton, Kiseleva & Hut 1998, see Naoz 2016 for the complete set of equations). We also include the effects of stellar evolution on stellar radii and masses, following the stellar evolution code SSE by Hurley, Pols & Tout (2000). The interaction between the EKL mechanism and post-main-sequence stellar evolution has been demonstrated to play an important role in three-body dynamical evolution (see Perets & Kratter 2012; Shappee & Thompson 2013; Michaely & Perets 2016; Naoz et al. 2016; Stephan et al. 2016; Toonen et al. 2016; Stephan et al. 2017, 2018).

2.2 Numerical set-up

We divide the parameter space into a grid in which we choose among a set of initial values for the masses of the three bodies (M_{VHya}, m_1, m_2), the semimajor axes of the inner and outer orbits

(a_1, a_2), the eccentricities of the inner and outer orbits (e_1, e_2), and the inclination (i) between the two orbits.[1]

Based on SSE modeling, the Zero-Age Main Sequence (ZAMS) mass of V Hya (M_{VHya}) was set to 2.2 M$_\odot$, appropriate for a carbon star. Each system is integrated for 1.2 Gyr unless a stopping condition is fulfilled. To allow for comparison with the observed system, we focus on the Late-AGB phase (L-AGB, i.e. 1.143–1.146 Gyr for the chosen mass) and determine whether the periastron of the inner orbit reaches the primary's Roche limit without merging. The Roche limit of V Hya is defined as (e.g. Paczyński 1971; Matsumura, Peale & Rasio 2010; Naoz 2016):

$$RL_{VHya} = q\,R_{VHya} \left(\frac{M_{VHya} + m_1}{M_{VHya}} \right)^{1/3} \qquad (1)$$

where q is a numerical factor of order unity. However, the radius of an AGB star is not well defined; its stellar envelope can extend to large distances, perhaps filling its own Roche limit. Thus, it is reasonable to assume that mass accretion can occur when the inner companion reaches the primary's Roche limit. We note that the parameter q is rather uncertain, in particular for a bound eccentric case. Numerical simulations have suggested that this parameter can be about 2.7 (e.g. Guillochon, Ramirez-Ruiz & Lin 2011; Liu et al. 2013), and that value may be a lower limit. Other studies sometimes find and adopt a smaller value ($q \sim 1.4$–1.6; e.g. Paczyński 1971). Thus, here, we explore two limiting cases, one for which $q = 1.66$, as was adopted in Naoz, Farr & Rasio (2012), and another for which $q = 2.7$, adopted in Petrovich (2015). These two limiting cases represent two different physical pictures: interactions with an extended envelope ($q = 2.7$) and a contained envelope ($q = 1.66$). The integration was stopped when the inner orbit pericenter $R_{p,1}$ reaches 80 per cent of V Hya's radius, R_{VHya}, i.e. $R_{p,1} \leq 0.8 R_{VHya}$.

We investigated a discrete range of initial values for m_1; a Neptune-sized planet (5×10^{-5} M$_\odot$), a Jupiter-sized planet (10^{-3} M$_\odot$), a brown dwarf (0.01 M$_\odot$), and a range of subsolar stellar companions (0.1, 0.3, 0.6, and 0.9 M$_\odot$). According to Sahai et al. (2016), the inner companion's mass should be sub-solar, thus we do not consider larger mass companions in our investigation.

The semimajor axis of the inner orbit (a_1) was set so that its period is 8.5 yr. We also note that it is unlikely that a planet around V Hya would have a high initial eccentricity. On the other hand, a stellar companion could have had a high initial eccentricity, but tides would have circularized its orbit by the time the primary entered the AGB phase. Thus, for the eccentricity of the inner companion, we adopt for simplicity an initial, almost circular orbit ($e_1 = 0.1$).

There is a degeneracy between m_2, a_2 and e_2 that comes from the Kozai time-scale (e.g. Naoz 2016):

$$t_{quad} \propto \frac{a_2^2 \left(1 - e_2^2\right)^{3/2} \sqrt{M_{VHya} + m_1}}{a_1^{3/2} m_2}. \qquad (2)$$

and therefore we can restrict these parameters to a narrow range of values because this time-scale must be shorter than the lifetime of V Hya. However, if m_2 is larger than m_1, the system dynamics can be described well by a test particle approximation ($m_2 \gtrsim 7m_1$; Teyssandier et al. 2013). In this case, the inner orbit can reach extreme eccentricities in very short time-scales (e.g. Li et al. 2014a,b). Thus, we do not expect differences in the evolution of

---

[1]Throughout this paper, we use the subscripts 1 and 2 to indicate the values for the inner and outer orbits of the system, respectively. For the mass parameter, the subscripts indicate V Hya (M_{VHya}), the inner companion (m_1) and the outer body (m_2).

Table 1. Grid of initial conditions for our 3-body model. A combination of all of these values gives a set of 2625 initial conditions. Parameters marked with an (*) were set the same for all computations. The semimajor axis of the inner orbit for each m_1 was calculated via $a_1 = (P_1^2(M_{\mathrm{VHya}} + m_1))^{1/3}$.

Parameter	Initial values
M_{VHya}*	2.2 (in $M_\odot$)
m_1	5×10^{-5}, 0.001, 0.01, 0.1, 0.3, 0.6, 0.9 (in $M_\odot$)
m_2	0.01, 0.1, 0.3, 0.6, 0.9 (in $M_\odot$)
a_1*	Set such that $P_1 = 8.5$ yrs ($\sim 5-6$ au)
a_2	200, 400, 600, 800, 1000 (in au)
e_1*	0.1
e_2	0.3, 0.45, 0.6
i	35, 70 105, 140, 175 (in degrees)

systems for which $m_2 \gtrsim 7m_1$. We chose a lower limit of m_2 to be 0.01 $M_\odot$ (a brown dwarf). As with m_1, we chose an upper limit of $m_2 = 0.9\,M_\odot$.

In the model we propose here, we assume that V Hya is part of a hierarchical triple system. This means that the value for a_2 must be much greater than a_1. Such a configuration allows us to use the secular approximation equations (Naoz 2016). Furthermore, a_2 needs to satisfy the following criterion for the secular approximation to be valid (e.g. Lithwick & Naoz 2011):

$$\epsilon = \frac{a_1}{a_2} \frac{e_2}{1 - e_2^2} < 0.1, \qquad (3)$$

where ϵ is a measure of the relative strengths of the octupole and quadrupole effects on the orbital dynamics. Therefore, we test a range of 200–1000 au in 200 au increments, with eccentricity values (e_2) of 0.3, 0.45, and 0.6.

Finally, we test a wide range of mutual orbit inclinations ($i = 35°-175°$ in $35°$ increments). Table 1 summarizes the parameters of our computations, which give a total of 2625 cases that were generated as initial conditions.

3 RESULTS

In this section we present the results from our 2625 simulated triple systems. We note that less than 1 per cent of our simulated systems were inconclusive, and thus we ignore those systems in our analysis.

We divide the simulations into 'survived' and 'merged' systems. We show examples in Fig. 1, which presents the time evolution of the inner orbit's semimajor axis (red), periastron distance (blue), and V Hya's stellar radius (purple) and Roche limit (green and cyan dashed lines). The Late AGB phase is shaded in purple, which lasts for $\sim$3 Myr for the chosen initial value of $M_{\mathrm{VHya}} = 2.2\,M_\odot$.

(i) **Merged systems**: Here we include all systems in which the inner binary merged at any point of the evolution, which occurs in $\sim$37 per cent of all simulated cases (991/2625). These merged systems can be divided into two groups:

(a) **L-AGB mergers**: systems that merged during the L-AGB period (an example is shown in the middle panel of Fig. 1). These can happen via an EKL-induced high eccentricity (e.g. Shappee & Thompson 2013; Naoz & Fabrycky 2014; Stephan et al. 2018). Furthermore, because tides are highly sensitive to the stellar radius, the likelihood of a merger is increased at this stage of stellar evolution due to circularization and shrinking of the inner binary's orbit (e.g. Naoz 2016). These systems comprise $\sim$76 per cent of all mergers (752/991).

(b) **Pre-AGB mergers**: systems that merged in previous stages of the stellar evolution of V Hya (right-hand panel of Fig. 1). These occur due to strong EKL effects due to stellar-mass inner and outer companions, as well as strong tidal interactions between the inner binary members. Such systems are likely to give rise to blue stragglers (e.g. Perets & Fabrycky 2009; Naoz & Fabrycky 2014). These systems comprise $\sim$24 per cent of all mergers (752/991).

(ii) **Survived binary systems**: Here we include systems in which the inner companion survives the evolution of V Hya without merging. This occurs in $\sim$62 per cent of all simulated cases (1616/2625). In these systems, the semimajor axis of the inner orbit increases substantially at $\sim$1.146 Gyr, which is when the star sheds its outer layers and becomes a white dwarf. Most of these systems are 'no interaction' systems, in which the inner companion survives the evolution of V Hya without interacting with the primary's Roche limit (an example of such a system in shown in the left-hand panel of Fig. 1). In general, these are systems in which EKL effects were insufficient to induce high eccentricities due to, for example, nearly coplanar orbits[2] ($i = 35$ or 175 deg, such as the example in the left-hand panel of Fig. 1), high a_2 values, or ratios $m_2/m_1 \approx 1$. However, there are also systems where EKL effects did increase the inner orbit's eccentricity, but not enough to make the inner orbit's periastron cross the primary's Roche limit (see Fig. 3). Our investigation focuses on the subset of surviving systems in which the inner companion's periastron reaches the primary's Roche limit during the L-AGB phase. These occur in $\sim$8 per cent of all cases (examples of these systems' orbital evolution are shown in Fig. 2), and can be further divided into two subcategories:

(a) **'Grazing' systems**: where the inner companion's orbit reaches a high eccentricity ($e_1 > 0.1$) and crosses the primary's Roche limit during its periastron passage (examples are shown in the left-hand and middle panels of Fig. 2). This configuration is maintained for $\sim$1 Myr until the primary becomes a white dwarf, at which point the inner companion's orbit increases and exits the Roche limit. During this 1 Myr period, $M_{\mathrm{VHya}} \sim 1.5-1.7\,M_\odot$, and $R_{\mathrm{VHya}} \sim 1.6$ au. In this configuration, the inner companion could, in principle, accrete material during its periastron passage. Then V Hya-like ejections could be produced by a transient accretion disc. The number of systems in this category depends on q. For $q = 2.7$, this condition is satisfied in $\sim$9 per cent of surviving systems (138/1616), while it is satisfied in only $\sim$2 per cent of surviving systems (27/1616) for $q = 1.66$.

(b) **'Temporary close binaries' (TCBs)**: systems where the inner companion's orbit circularizes during the Late-AGB phase and is engulfed by V Hya's Roche limit, but does not lead to a merger with the latter (an example is shown in the right-hand panel of Fig. 2). We call these systems 'temporary close binaries'. This condition is only satisfied using a factor of $q = 2.7$ in the definition of the Roche limit, and in $\sim$4 per cent of surviving systems (60/1616). While these cases could not produce V Hya-like systems, they are likely to end up as common envelope configurations because of the drag encountered inside the Roche limit.[3]

---

[2]Coplanarity does not guarantee a small eccentricity excitation, as was shown in Li et al. (2014a).

[3]Drag forces also affect the grazing systems we describe above. To determine whether the primary's extended envelope significantly affects the grazing companion's orbit is equivalent to asking whether the orbital average is
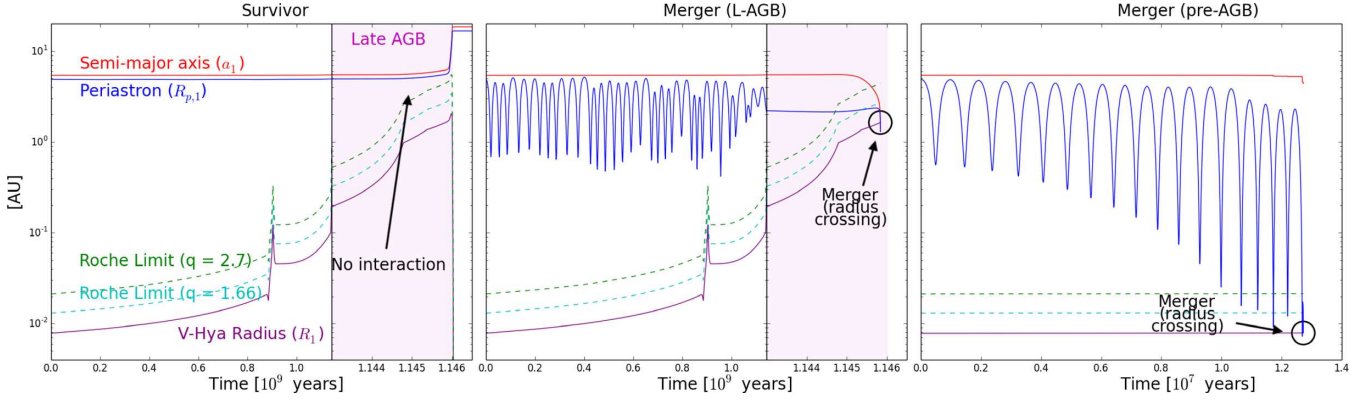
Figure 1. Example of orbital evolutions of survivor and merger systems. The purple-shaded region indicates the Late-AGB phase, which lasts for ~ 3 Myr. *Left*: system in which the inner companion's periastron (blue line) never crosses V Hya's Roche limit (green-dashed line). The semi-major axis of the inner orbit (red line) increases substantially at ~ 1.146 Gyr. This is because at this time the star sheds most of its mass and becomes a white dwarf. Initial system parameters for this system are $m_1 = 0.001$ M$_\odot$, $m_2 = 0.01$ M$_\odot$, $a_2 = 400$ au, $e_2 = 0.3$, $i = 175$ deg. *Middle*: system in which the inner companion merges with V Hya during the L-AGB phase. Initial system parameters are $m_1 = 0.001$ M$_\odot$, $m_2 = 0.01$ M$_\odot$, $a_2 = 200$ au, $e_2 = 0.45$ $i = 70$ deg. *Right*: system in which strong EKL oscillations of the inner orbit's periastron prompts the companion to merge with V Hya during the Main Sequence phase. Initial system parameters are $m_1 = 0.01$ M$_\odot$, $m_2 = 0.3$ M$_\odot$, $a_2 = 200$ au, $e_2 = 0.6$, and $i = 70$ deg.
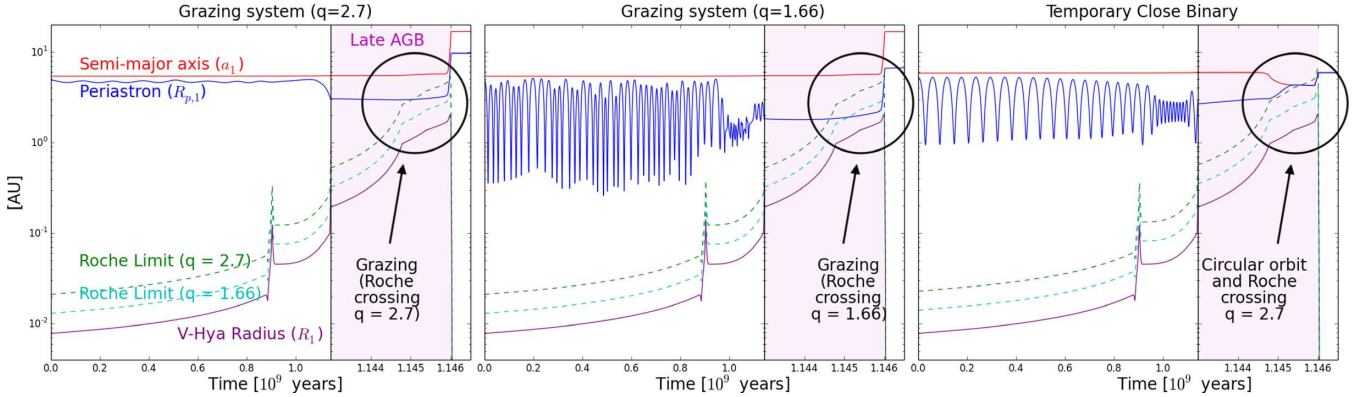
Figure 2. Example orbital evolutions of 'grazing' systems. The purple-shaded region indicates the Late-AGB phase, which lasts for ~ 3 Myr. *Left*: system in which the inner companion's periastron (blue line) crosses V Hya's Roche limit (green dashed line, $q = 2.7$) during the L-AGB phase. Initial system parameters are $m_1 = 0.001$ M$_\odot$, $m_2 = 0.01$ M$_\odot$, $a_2 = 400$ au, $e_2 = 0.6$, $i = 105$ deg. *Middle*: system in which the inner companion's periastron (blue line) crosses V Hya's Roche limit (cyan dashed line, $q = 1.66$) during the L-AGB phase. Initial system parameters are $m_1 = 5 \times 10^{-5}$ M$_\odot$, $m_2 = 0.01$ M$_\odot$, $a_2 = 200$ au, $e_2 = 0.6$, $i = 35$ deg. *Right*: system in which the inner companion's orbit circularizes, and its semimajor axis (red line) crosses the Roche limit of V Hya (green dashed line, $q = 2.7$). Initial system parameters are $m_1 = 0.6$ M$_\odot$, $m_2 = 0.6$ M$_\odot$, $a_2 = 1000$ au, $e_2 = 0.6$, $i = 70$ deg.

We show in Fig. 3 how the mass of the inner companion (m_1) affects the evolution of the system. In the left-hand panel we illustrate the relationship between D_{min} and eccentricity. We define D_{min} as

$$D_{min} = \min[(a_1(1 - e_1)) - RL_{VHya}], \qquad (4)$$

valid in the secular approximation, compared to the orbital (or less than orbital) effects due to the drag force. In other words, if on an orbital time-scale the companion's velocity is changing significantly, then the secular approximation is invalid. So the question boils down to which force dominates over the orbital time-scale (the EKL produces forced eccentricity that remains constant over the entire ~ 1 Myr in which the companion's periastron grazes the Roche limit of V Hya). Estimating the drag force as $F_{drag} \approx 0.5\rho\pi R_1^2 v_1^2$, using $\rho = 10^{-8}$ g cm^{-3} (Lagadec et al. 2005), we a find very small change in velocity of the grazing companions (Jovians and brown dwarf-mass companions) due to the drag force (< 1 per cent) over one orbit, the velocity will have been re-established by EKL again.

i.e. the minimum distance between the periastron of the inner orbit and V Hya's Roche limit ($D_{min} = 0$ indicates Roche limit crossing, using $q = 2.7$). On the *x*-axis, we show the eccentricity at the time of D_{min} ($t_{D_{min}}$, which occurs during the L-AGB phase). It is clear that most surviving stellar companions ($m_1 > 0.1$ M$_\odot$) circularize (reach final values of $e_1 \sim 0$). This is because stellar companions have larger radii than lower-mass objects, and since tides are highly dependent on the radius, their orbits circularize relatively quickly. Because of the relatively larger mass of stellar objects, the EKL mechanism isn't as effective since the distant tertiary has lower or similar mass.

Most companions with $m_1 = 0.1$ M$_\odot$ merge during or before the L-AGB phase, as indicated in the right-hand panel of Fig. 2. Most of the TCB systems contain a stellar mass $m_1 > 0.1$ M$_\odot$ companion, while brown dwarfs and planets ($m_1 < 0.1$ M$_\odot$) produce mainly grazing systems.

Most surviving non-stellar companions ($m_1 < 0.1$ M$_\odot$, i.e. Jovians and Brown dwarfs) follow a linear relation between D_{min}
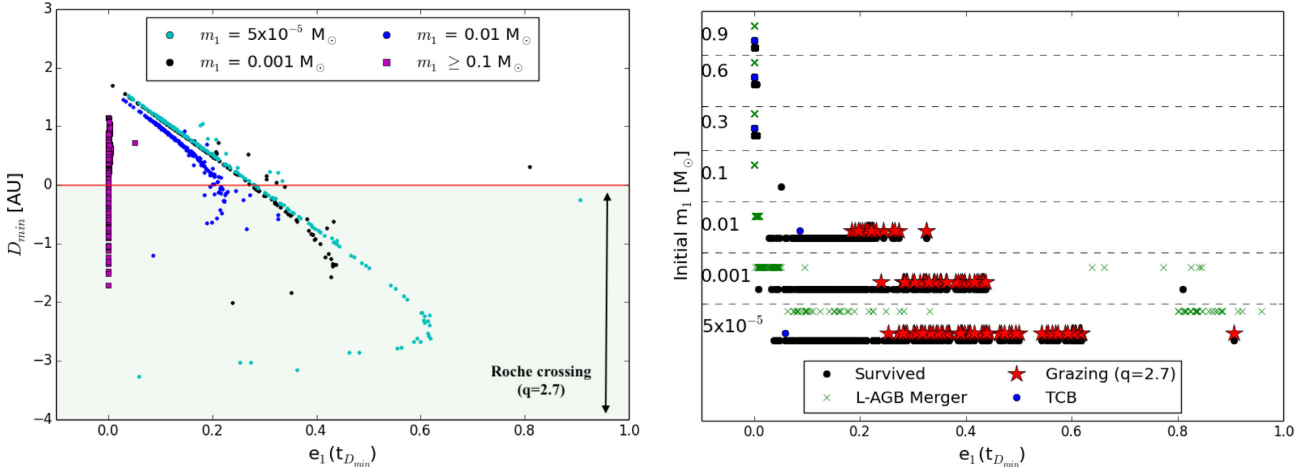
Figure 3. Illustration of how the end state of the system depends on the mass of the inner companion (m_1). *Left*: Plot of D_{min} (equation 4) versus the eccentricity of the inner orbit (e_1) at the time of minimum periastron distance to the primary's Roche limit ($t_{D\mathrm{min}}$, using $q = 2.7$). We do not include any merger system in this panel. Green-shaded region represents the Roche limit crossing. *Right*: Plot of outcomes as a function of initial m_1 versus and eccentricity of the inner orbit (e_1) at the time of minimum periastron distance to the primary's Roche limit ($t_{D\mathrm{min}}$, using $q = 2.7$). Stellar-mass ($m_1 > 0.1$ M$_\odot$, and a few planets) companions produce TCBs (blue dots), while planets (and brown dwarfs, all with $m_1 < 0.1$ M$_\odot$) produce grazing systems (red stars). Neptune-mass objects achieve the highest eccentricities. Green crosses (x) represent L-AGB mergers, and black dots (●) represent survivor systems (like those in the left-hand panel of Fig. 1).

and $e_1(t_{D\mathrm{min}})$. There is also a subtle mass dependence (see Fig. 3): lower-mass objects reach higher eccentricities. Using the upper limit value of $q = 2.7$, our simulations show that among all the objects that end up grazing the primary's Roche limit, there are more Neptune-mass objects than any other, followed by Jupiter-mass and brown dwarf companions. This is due to the fact that, for larger m_2/m_1 ratios, EKL effects approach the test particle approximation, in which the inner orbit achieves very high eccentricities. Moreover, tides become less effective for inner companions with small radii. Therefore, systems with Neptune-mass inner companions can graze V Hya's Roche limit with the highest eccentricities without being significantly affected by tidal forces.

We now examine constraints on the mass of the third, more distant companion, as well as its eccentricity and semimajor axis. Fig. 4 shows the percentage of grazing systems (relative to the total number of grazing brown dwarfs, Jupiters, and Neptunes) that contain different values of m_2, a_2, and e_2. Our results indicate that most grazing Neptunes were caused by far away ($a_2 \sim 800$–1000 au), sub-solar mass companions ($m_2 > 0.1$ M$_\odot$; see the middle panel of Fig. 4). This is expected because a less massive tertiary would be torqued by m_1 (e.g. Naoz 2016; Naoz et al. 2017). Thus, a more massive m_2 is an expected consequence of the EKL mechanism. On the other hand, grazing brown dwarfs are more likely to take place for systems in which the tertiary is closer (as shown in Fig. 4, right-hand panel). This is also an expected consequence of the EKL mechanism (e.g. Naoz 2016). In this case, the ratio m_2/m_1 is smaller than those systems with Neptune-mass inner companions, and thus we need a closer tertiary for EKL effects to induce high eccentricities.

4 IMPLICATIONS FOR THE V HYA SYSTEM

4.1 Observational interpretation of the orbit

The model introduced by Sahai et al. (2016) suggests that the observed ejections from V Hya are associated with the periastron passage of an unseen companion in an eccentric orbit. Furthermore,

their study suggested that the eccentricity of the companion has to be relatively large, $e \gtrsim 0.6$, in order for the companion to approach the primary within its stellar envelope at periastron.

However, here we relax the need for the companion to reach V Hya's radius, since crossing the Roche limit already provides an opportunity for interactions between V Hya and the companion. Furthermore, the low surface gravity, stellar pulsations, and their associated shocks, coupled with the radiation pressure that drives V Hya's stellar wind cause an increased scale height of its atmosphere, and therefore a measurable radius is not clearly definable (Zhao-Geisler et al. 2012).

4.2 Launching mechanism

The launching mechanism of the observed bullet ejections is largely uncertain. Here we consider the consequences of a few simple proof-of-concept launching mechanisms on our proposed scenario.
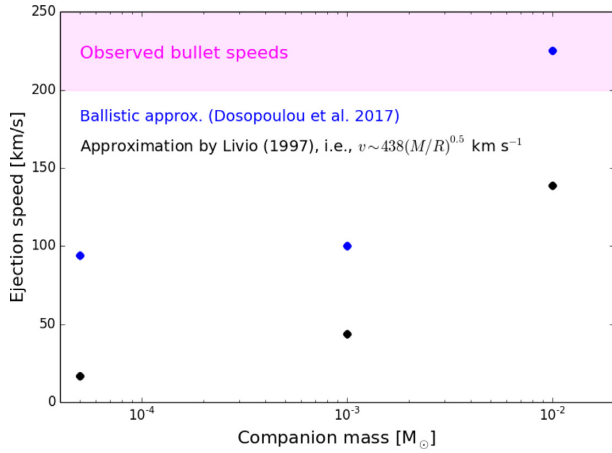
(i) The ballistic approximation (e.g. Dosopoulou, Naoz & Kalogera 2017) yields that the bullet speed v_b should be proportional to the periastron speed v_p plus the escape speed from the companion v_{esc}, i.e.

$$v_b \sim \sqrt{G(M_{\mathrm{VHya}} + m_c)\frac{1+e}{a(1-e)}} + \sqrt{\frac{2Gm_c}{r_c}} \quad (5)$$

where m_c is the mass of the companion and r_c is its radius. A similar estimation was done by Livio (1997). As can be seen from equation (5), the jet's velocity is highly sensitive to the mass of the companion. In our case, each companion reaches different maximum eccentricity (see Fig. 3), however the pericenter velocity is typically much smaller than the escape velocity. In Fig. 5 we show ejection speed according to these approximations for different companions (Neptune, Jupiter, and brown dwarf). A brown dwarf gives an ejection speed of about 230 km s^{-1}, similar to the observed bullet speeds ($v \sim 200$–250 km s^{-1}; Sahai et al. 2016; Scibelli, Sahai & Morris 2019).
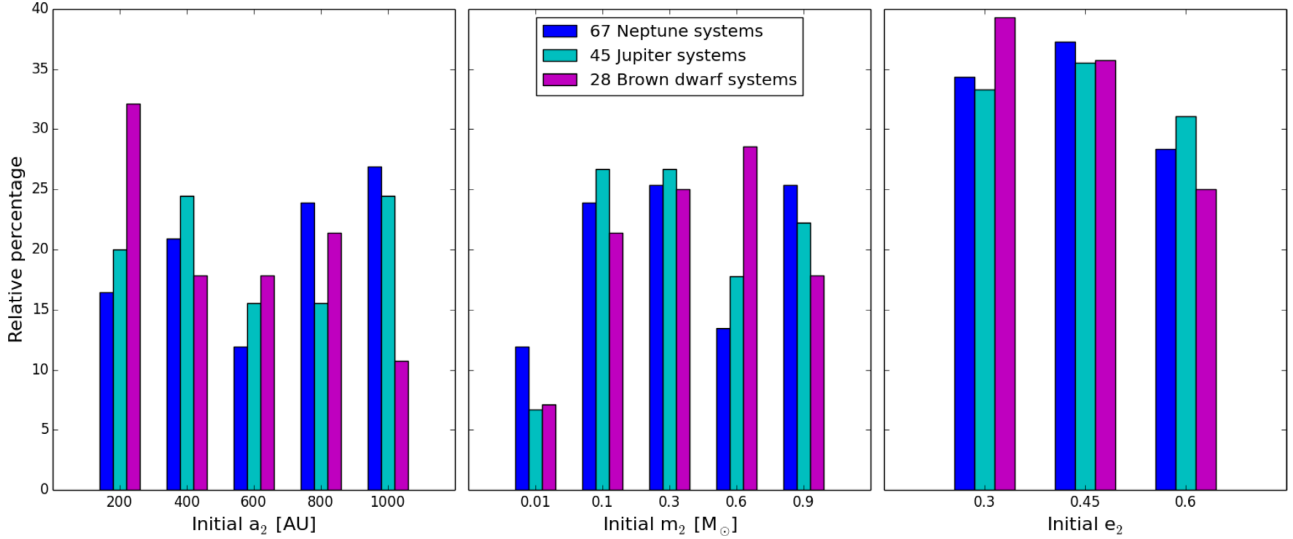
Figure 4. Percentages of Neptune, Jupiter, and brown dwarf systems (relative to total of grazing systems) for the values of m_2, a_2, and e_2. For example, in 33 per cent out of 28 systems with a brown dwarf (i.e. 9 systems), the location of m_2 is 200 au.

Figure 5. Jet ejection speed versus companion mass (for Neptune, Jupiter, and brown dwarf masses). Black dots represent the approximation by Livio (1997). The blue dots represent the ballistic approximation (Dosopoulou et al. 2017). The magenta-shaded region indicates the range of the observed bullets' speeds.

(ii) We also consider a magnetically driven launching mechanism. Following Fendt (2003), we consider an outflow velocity from a circum-planetary accretion disc:

$$v_b \approx 63 \text{ km s}^{-1} \left(\frac{\Phi}{5 \times 10^{22} \text{ G cm}^2} \right)^{2/3} \left(\frac{P}{4 \text{ d}} \right)^{-2/3}$$
$$\times \left(\frac{\dot{M}_{\text{out}}}{10^{-3} \dot{M}_{\text{in}}} \right)^{-1/3} \left(\frac{\dot{M}_{in}}{6 \times 10^{-5} \text{ M}_{\text{J}}/\text{yr}} \right)^{-1/3} \quad (6)$$

where Φ is the magnetic flux through the accretion disc, P is the outer edge disc's period, $\dot{M}_{\text{in}}$ is the inflow rate, and $\dot{M}_{\text{out}}$ is the outflow rate. If the companion swings through V Hya's Roche limit and forms a transient accretion disc,[4] we might expect ejections due to magnetically driven jets. This mechanism is sensitive to

the magnetic field of the system. For example, some studies have suggested that Jupiter's magnetic field could have been as high as $\sim$ 500 G during its early formation period (Christensen, Holzwarth & Reiners 2009; Batygin 2018). Furthermore, one version of the model we propose here, i.e. a Jovian planet around V Hya, might resemble the environment of a protoplanetary system, and thus, we could consider magnetic field strengths of 500 G or greater. Similar to Fendt (2003), we adopt $10 \times R_c$ as the outer disc edge. We also adopt $\dot{M}_{\text{out}} = \dot{M}_{\text{in}}$, i.e. all of the accreted mass is ejected. In Fig. 6 we show the ejection speed as a function of mass accretion rate, using values of $B = 500$ and 2000 G. As shown in the figure, accretion rates of $\sim 10^{-7}$ M$_\odot$/yr and a strong magnetic field ($B = 2000$ G) are necessary for a Jovian planet to cause ejection speeds of $\sim$200 km s^{-1}.

(iii) Another launching mechanism is described in Goodson & Winglee (1999). In their work, they considered accretion jets from accreting magnetic young stellar objects. They found that the ejection speeds are

$$v_b = 585 P_d^{-2/3} B_{kG}^{2/3} R^{4/3} \dot{M}_8^{-1/3} \sin^{4/3}\theta_{\text{jet}} \text{ km s}^{-1} \quad (7)$$

where P_d is the stellar rotation period in days, B_{kG} is the stellar surface magnetic field in kilogauss, R is the stellar radius in solar radii, $\dot{M}_8$ is the jet mass flux in units of 10^{-8} M$_\odot$/yr, and θ_{jet} is the angle of ejection. For simplicity, we assume $\sin\theta_{\text{jet}} = 1$, and a maximally rotating Jovian planet ($P_d \approx 0.2$ d). We consider the same values of B and $\dot{M}_{\text{in}}$ as before, and show the resulting jet speed values in Fig. 6. The speeds resulting from this mechanism are lower than those produced using equation (6).

4.3 Relevance for companions around evolved stars

In recent years a number of evolved stars have been observed to host Hot Jupiter companions (e.g. Johnson et al. 2008; Sato et al. 2008; Johnson et al. 2010, 2011a,b; Johnson, Morton & Wright 2013; Sato et al. 2013; Bieryla et al. 2014; Wittenmyer et al. 2015a,b).

---

[4]Note that the time-scales to form an accretion disk ($t \sim (G\rho)^{-1/2} \sim 1.2$ yr) is too long compared to the few months the companion typically spends inside

the Roche limit. However, an accretion disc might be accumulated over one or more orbital revolution time-scale.
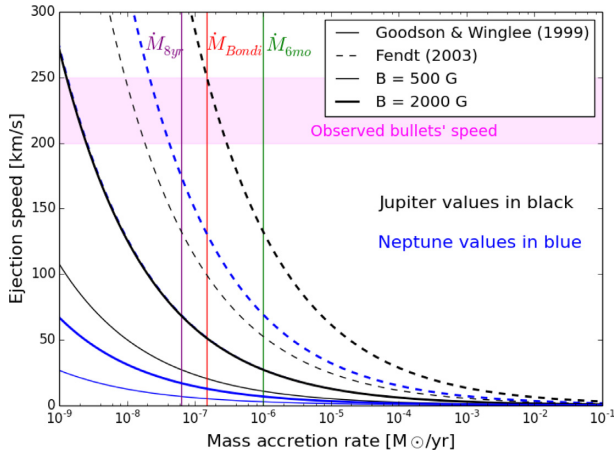
Figure 6. Plot of ejection speed versus mass input rate. Solid lines represent ejection speed values according to equation (7) (Goodson & Winglee 1999). Dashed lines represent values according to equation (6) (Fendt 2003). Black lines represent values due to a Jupiter planet, while blue lines represent values for a Neptune planet. Thicker lines represent values with $B = 2000$ G, while thinner lines represent values with $B = 500$ G. We also indicate some possible values of the mass accretion rate ($\dot{M}_{in}$). The vertical purple line indicates the value due to the accretion of 1 bullet mass ($\sim 10^{27}$ g, Sahai et al. 2016) over 1 orbit (8 yr). Similarly, the vertical green line indicates the rate of accretion of 1 bullet mass over 6 months. The vertical red line represents Bondi accretion, assuming a density $\rho \sim 10^{-8}$ g cm^{-3} (estimate taken from Lagadec et al. 2005).

Recent work by Stephan et al. (2018) indicates the existence of a population of 'Temporary Hot Jupiters' (THJs), of which V Hya's unseen companion could be an example. In this model, a giant planet orbiting its parent star at a significant distance is perturbed by an outer stellar companion to reach high eccentricity values. Once the parent star becomes a red giant, tidal forces bring the planet closer, becoming Hot Jupiters until they are eventually engulfed by the expanding star. However, our model here suggests that a subset of these THJs would in fact become V Hya-like systems when they begin to interact with the expanding star's extended envelope. It can, thus, be speculated that a number of observed Hot Jupiters orbiting evolved stars are indeed progenitors of future V Hya-like objects.

5 SUMMARY

In this paper, we propose a dynamical configuration for the AGB star, V Hya, that accounts for its apparently periodic 'bullet' ejections. In our model, V Hya is part of a hierarchical triple system. The inner, 8.5-yr period orbit is composed of V Hya and a low-mass companion, and they are orbited by a distant tertiary. We have evolved a large set (2625) of realizations of this system, varying the masses, as well as the orbital separations, eccentricities, and inclinations of the system. Our goal is to constrain the parameter space for which a V Hya-like system can occur. We include the EKL mechanism, tides, general relativity, and post-main-sequence stellar evolution. The eccentricity oscillations associated with the EKL mechanism can potentially drive the inner companion to cross inside the primary's Roche limit. Such an interaction could produce jet-like ejections via a strongly enhanced accretion episode.

Our results can be summarized as follows:

(i) **Mergers**. In ~37 per cent of all simulated cases, the inner companion merges with the primary, either due to strong tides during the primary's Late AGB phase, or due to extreme EKL effects that lead to a merger before the AGB phase.

(ii) **Surviving systems**. In ~62 per cent of the simulated systems, the inner companion survives the evolution of the primary star until its WD phase without merging. Our investigation focuses on the subset of these cases that achieves Roche-limit crossing at periastron during the primary's Late AGB phase.

(iii) **Late-AGB, grazing systems**: cases that could potentially give rise to a V Hya-like system. In these systems, the inner companion's orbit reaches a high eccentricity ($e_1 > 0.1$) during the primary's Late-AGB phase and crosses the primary's Roche limit during periastron passage. Thus, the inner companion could, in principle, accrete material during this period. The percentage of systems in this category depends on the properties of the evolved star's envelope as well as the details of the interactions of the close-by companion with the Roche limit (Guillochon et al. 2011; Liu et al. 2013). We characterize this by adopting two different numerical pre-factors for the Roche limit. Specifically, in equation (1), we find that for $q = 2.7$ ($q = 1.66$), ~5 per cent (~1 per cent) of all simulated systems may become V Hya-like systems. It is not surprising that only small percentage of the systems present this behavior as we are constraining ourselves to a very short time-scale in the evolution of the star (the Late-AGB phase represents 1/400 of our simulation time-scale). Grazing systems only occur with brown dwarfs, Jupiter, and Neptune-mass inner companions (Fig. 3). We can then estimate a possible mass and semimajor axis of the distant tertiary (Fig. 4). For example, we find more systems with a brown dwarf inner companion and a relatively close ($a_2 \sim 200$ au), stellar-mass ($m_2 \sim 0.6$ M$_\odot$) tertiary.

(iv) **Late AGB, temporary close binaries (TCBs)**. Unlike the systems in which their orbit circularizes and shrinks, in TCBs tides work to circularize the inner orbit during the primary's Late AGB phase, and the secondary migrates inside the primary's Roche limit, but a merger does not occur. Specifically, the mass-loss expands the semimajor axis, which helps the companion elude engulfment. We find these systems only when using a value of $q = 2.7$ in the definition of the Roche limit, and in ~2 per cent of all cases we analyzed. While these cases would not produce V Hya-like systems, they are likely to end up as common envelope configurations because of the drag encountered inside the Roche limit. Most systems in this category contain stellar-mass inner companions ($m_1 > 0.1$ M$_\odot$).

Finally, we consider some possible launching mechanisms that could give rise to V Hya-like ejections. In particular, we examine a simple ballistic approach, as well as magnetically driven ejection processes that were suggested in the literature for proto-planetary systems and young stellar objects. Interestingly, we find (Fig. 5) that a simple ballistic mechanism can produce the observed ejection velocity for a brown dwarf companion. However, this version of our model causes tension with the companion's suggested eccentricity ($e_1 > 0.6$; Sahai et al. 2016), since our results indicate that tidal effects may limit a brown dwarf companion's eccentricity below ~0.2. Note that Sahai et al. (2016) suggested an eccentricity that was based on the companion approaching V Hya's envelope at periastron ($R_{VHya} \sim 2$ au). We relax this condition in our investigation.

Nevertheless, our results indicate that Jovian companions achieve the highest eccentricities during V Hya's Late AGB phase ($e_1 \sim 0.6$ for Neptune-mass companions, in agreement with the eccentricity suggested by Sahai et al. 2016). Here, a purely ballistic ejection does not produce speeds that match observations. Instead, a strong magnetic field ($B > 500$ G) is necessary for magnetically driven outflows

from a Jovian companion to achieve speeds of $\gtrsim 200 \, \text{km s}^{-1}$ (Fig. 6). This prediction can be used to distinguish competing mechanisms.

This proof-of-concept study suggests that V Hya-like ejections can result from EKL-induced interactions between AGB stars and Jovian or brown dwarf companions. The model presented here also provides a framework to explain the dynamics occuring in interacting binary systems in which the companion is a stellar, sub-stellar, or planetary object. This includes, for example, planets engulfed by giant stars (e.g. Soker, Livio & Harpaz 1984; Livio & Soker 2002; Gaudi et al. 2017; Stephan et al. 2018), the influence of planets on horizontal giant branch morphology (e.g. Soker 1998a), as well as binary progenitor models of bipolar PNe (e.g. Morris 1987; Soker 1998b).

REFERENCES

Balick B., Frank A., 2002, ARA&A, 40, 439
Batygin K., 2018, AJ, 155, 178
Bieryla A. et al., 2014, AJ, 147, 84
Christensen U. R., Holzwarth V., Reiners A., 2009, Nature, 457, 167
Dosopoulou F., Naoz S., Kalogera V., 2017, ApJ, 844, 12
Eggleton P. P., Kiseleva L. G., Hut P., 1998, ApJ, 499, 853
Eggleton P. P., Kisseleva-Eggleton L., Dearborn X., 2007, in Hartkopf W. I., Harmanec P., Guinan E. F., eds, IAU Symp. Vol. 240, Binary Stars as Critical Tools and Tests in Contemporary Astrophysics. Kluwer, Dordrecht, p. 347
Fendt C., 2003, A&A, 411, 623
Gaudi B. S. et al., 2017, Nature, 546, 514
Goodson A. P., Winglee R. M., 1999, ApJ, 524, 159
Griffin R. F., 2012, JA&A, 33, 29
Guillochon J., Ramirez-Ruiz E., Lin D., 2011, ApJ, 732, 74
Hirano N. et al., 2004, ApJ, 616, L43
Hurley J. R., Pols O. R., Tout C. A., 2000, MNRAS, 315, 543
Hut P., 1980, A&A, 92, 167
Johnson J. A. et al., 2011a, AJ, 141, 16
Johnson J. A. et al., 2011b, ApJS, 197, 26
Johnson J. A., Marcy G. W., Fischer D. A., Wright J. T., Reffert S., Kregenow J. M., Williams P. K. G., Peek K. M. G., 2008, ApJ, 675, 784
Johnson J. A., Howard A. W., Bowler B. P., Henry G. W., Marcy G. W., Wright J. T., Fischer D. A., Isaacson H., 2010, PASP, 122, 701
Johnson J. A., Morton T. D., Wright J. T., 2013, ApJ, 763, 53
Knapp G. R., Jorissen A., Young K., 1997, A&A, 326, 318
Kozai Y., 1962, AJ, 67, 591
Lagadec E., Mékarnia D., de Freitas Pacheco J. A., Dougados C., 2005, A&A, 433, 553
Li G., Naoz S., Kocsis B., Loeb A., 2014a, ApJ, 785, 116
Li G., Naoz S., Holman M., Loeb A., 2014b, ApJ, 791, 86

Lidov M. L., 1962, Planet. Space Sci., 9, 719
Lithwick Y., Naoz S., 2011, ApJ, 742, 94
Liu S.-F., Guillochon J., Lin D. N. C., Ramirez-Ruiz E., 2013, ApJ, 762, 37
Livio M., 1997, in Wickramasinghe D. T., Bicknell G. V., Ferrario L., eds, ASP Conf. Ser. Vol. 121, IAU Colloq. 163: Accretion Phenomena and Related Outflows. Astron. Soc. Pac., San Francisco, p. 845
Livio M., Soker N., 2002, ApJ, 571, L161
Lloyd Evans T., 1991, MNRAS, 248, 479
Matsumura S., Peale S. J., Rasio F. A., 2010, ApJ, 725, 1995
Michaely E., Perets H. B., 2016, MNRAS, 458, 4188
Morris M., 1987, PASP, 99, 1115
Naoz S., 2016, ARA&A, 54, 441
Naoz S., Fabrycky D. C., 2014, ApJ, 793, 137
Naoz S., Farr W. M., Rasio F. A., 2012, ApJ, 754, L36
Naoz S., Farr W. M., Lithwick Y., Rasio F. A., Teyssandier J., 2013a, MNRAS, 431, 2155
Naoz S., Kocsis B., Loeb A., Yunes N., 2013b, ApJ, 773, 187
Naoz S., Fragos T., Geller A., Stephan A. P., Rasio F. A., 2016, ApJ, 822, L24
Naoz S., Li G., Zanardi M., de Elía G. C., Di Sisto R. P., 2017, AJ, 154, 18
Paczyński B., 1971, ARA&A, 9, 183
Perets H. B., Fabrycky D. C., 2009, ApJ, 697, 1048
Perets H. B., Kratter K. M., 2012, ApJ, 760, 99
Petrovich C., 2015, ApJ, 799, 27
Pribulla T., Rucinski S. M., 2006, AJ, 131, 2986
Prodan S., Antonini F., Perets H. B., 2015, ApJ, 799, 118
Raghavan D. et al., 2010, ApJS, 190, 1
Sahai R., Trauger J. T., 1998, AJ, 116, 1357
Sahai R., Morris M., Knapp G. R., Young K., Barnbaum C., 2003, Nature, 426, 261
Sahai R., Sugerman B. E. K., Hinkle K., 2009, ApJ, 699, 1015
Sahai R., Morris M. R., Villar G. G., 2011, AJ, 141, 134
Sahai R., Scibelli S., Morris M. R., 2016, ApJ, 827, 92
Sato B. et al., 2008, PASJ, 60, 539
Sato B. et al., 2013, PASJ, 65, 85
Scibelli S., Sahai R., Morris M. R., 2019, ApJ, 870, 117
Shappee B. J., Thompson T. A., 2013, ApJ, 766, 64
Soker N., 1998a, AJ, 116, 1308
Soker N., 1998b, ApJ, 496, 833
Soker N., Livio M., Harpaz A., 1984, MNRAS, 210, 189
Stephan A. P., Naoz S., Ghez A. M., Witzel G., Sitarski B. N., Do T., Kocsis B., 2016, MNRAS, 460, 3494
Stephan A. P., Naoz S., Zuckerman B., 2017, ApJ, 844, L16
Stephan A. P., Naoz S., Gaudi B. S., 2018, AJ, 156, 128
Teyssandier J., Naoz S., Lizarraga I., Rasio F. A., 2013, ApJ, 779, 166
Tokovinin A., 2008, MNRAS, 389, 925
Tokovinin A., 2014a, AJ, 147, 86
Tokovinin A., 2014b, AJ, 147, 87
Tokovinin A., Thomas S., Sterzik M., Udry S., 2006, A&A, 450, 681
Tokovinin A. A., 1997a, Astron. Lett., 23, 727
Tokovinin A. A., 1997b, A&AS, 124, 75
Toonen S., Hamers A., Portegies Zwart S., 2016, Comput. Astrophys. Cosmol., 3, 6
Wittenmyer R. A., Gao D., Hu S. M., Villaver E., Endl M., Wright D., 2015a, PASP, 127, 1021
Wittenmyer R. A., Wang L., Liu F., Horner J., Endl M., Johnson J. A., Tinney C. G., Carter B. D., 2015b, ApJ, 800, 74
Zhao-Geisler R., Quirrenbach A., Köhler R., Lopez B., 2012, A&A, 545, A56

This paper has been typeset from a TeX/LaTeX file prepared by the author.